

Addressing the Minor-Embedding Problem in Quantum Annealing and Evaluating State-of-the-Art Algorithm Performance

Aitor Gómez-Tejedor^{a,b}, Eneko Osaba^a, Esther Villar-Rodriguez^a

^aTECNALIA, Basque Research and Technology Alliance (BRTA), P. Tecnológico, Ed. 700, 48160 Derio, Spain

^bUniversity of the Basque Country (UPV/EHU), 48013 Bilbao, Spain

Abstract

This study addresses the minor-embedding problem, which involves mapping the variables of an Ising model onto a quantum annealing processor. The primary motivation stems from the observed performance disparity of quantum annealers when solving problems suited to the processor's architecture versus those with non-hardware-native topologies. Our research has two main objectives: *i*) to analyze the impact of embedding quality on the performance of D-Wave Systems quantum annealers, and *ii*) to evaluate the quality of the embeddings generated by Minorminer, an algorithm provided by D-Wave and widely recognized as the standard minor-embedding technique in the literature. Regarding the first objective, our experiments reveal a clear correlation between the average chain length of embeddings and the relative errors of the solutions sampled. This underscores the critical influence of embedding quality on quantum annealing performance. For the second objective, we focus on the Minorminer technique, assessing its capacity to embed problems, the quality of the embeddings produced, and the robustness of the results. We also compare its performance with Clique Embedding, another algorithm developed by D-Wave, which is deterministic and designed to embed fully connected Ising models into quantum annealing processors, serving as a worst-case scenario. The results demonstrate that there is significant room for improvement for Minorminer, as it has not consistently outperformed the worst-case scenario.

Keywords: Quantum Computing, Quantum Annealing, D-Wave, Graph Theory, Minor-embedding, Minorminer.

1. Introduction

Quantum computing (QC) is recognized as the next significant advancement in computing, with substantial potential across various fields, including combinatorial optimization. In this domain, QC can address problems in fundamentally different ways compared to classical methods, potentially offering significant advantages.

Despite its promising potential, we are currently in the *noisy intermediate scale quantum (NISQ)* [1] era, which means that the technology is still in early development and faces hardware limitations. These limitations include the poor quality of qubits, which causes undesirable behavior, and a reduced number of qubits and couplers (connections between pairs of qubits) in the processors. In spite of these restrictions, extensive research is being conducted on the software and algorithmic aspects of the paradigm. Much of this research aims to address these constraints and maximize the potential of current NISQ-era quantum computers. Examples of research areas within this category include the design of hybrid methods that integrate classical and quantum processors [2] [3] [4], as well as error correction and error mitigation techniques [5] [6].

Among the various types of quantum computers, the gate-model and quantum annealing are the most prominent. This

study focuses on the latter. Quantum annealing (QA) is grounded in the principles of adiabatic quantum computing, as initially proposed by Farhi et al. [7]. The adiabatic quantum computing paradigm starts by initializing a quantum system in an easy-to-prepare ground state. Then, the system's time-dependent Hamiltonian is slowly evolved within the adiabatic theorem [8] regime until its final form is reached, where the state desired to be computed is encoded as the ground state. By evolving the system slowly enough, the adiabatic theorem states that there is a high probability that the final state of the system will be the desired ground state. Quantum annealing modifies this approach by relaxing the requirement for slow evolution, which is dependent on the problem and can be exponentially large. This relaxation allows for faster execution times, albeit with a reduced probability of achieving the ground state.

There are different models for building quantum annealers, such as those based on Rydberg atoms [9], trapped ions [10] or superconducting flux qubits [11], with the latter being the most recognized to date. Additionally, several companies are working on this technology and building their own devices, such as NEC¹, Qilimanjaro², and D-Wave Systems³.

In the literature, the reference quantum annealers are those developed by D-Wave Systems, which are specifically designed to solve Ising models by sampling low-energy states of a given

Email addresses: aitor.gomez-tejedor@tecnalia.com (Aitor Gómez-Tejedor), eneko.osaba@tecnalia.com (Eneko Osaba), esther.villar@tecnalia.com (Esther Villar-Rodriguez)

¹<https://parityqc.com/a-new-quantum-annealer-by-nec>

²<https://qilimanjaro.tech>

³<https://www.dwavesys.com>

Hamiltonian in which the Ising model is encoded [12]. Consequently, these annealers forfeit the computational universality inherent in general quantum annealing. However, the Ising model is mathematically equivalent to solving a quadratic unconstrained binary optimization (QUBO) model, and many combinatorial optimization problems can be formulated as QUBOs [13], and therefore, as Ising models [14].

This study exhaustively analyzes the *minor-embedding* problem, a graph theoretical problem responsible for mapping the variables of the Ising model onto the quantum annealing processor. The motivation lies in the observed performance disparity of D-Wave’s processors when addressing hardware-native problems versus real-world optimization problems with generic topologies. Specifically, quantum annealers exhibit competitive performance with certain classical solvers when solving problems that are inherently suited to the processor’s architecture, thereby eliminating the need for minor-embedding, as shown in [15] and [16]. However, when applied to optimization tasks whose Ising model formulation has a non-hardware-native topology, the solution quality produced by quantum annealers is significantly inferior to that achieved by classical solvers [17] [18]. This disparity highlights the importance of the minor-embedding problem in the context of quantum annealing.

Furthermore, the mapping is not only critical but also highly complex to solve. The challenge arises from the limited connectivity of the processors, making the mapping of any Ising model non-trivial. In fact, the lower the hardware connectivity, the lower the likelihood that a problem can be trivially mapped onto the hardware. For instance, consider an Ising model where a variable interacts with 16 others, while the hardware qubits are only connected to 15 other qubits. This discrepancy hinders a direct one-to-one mapping of variables to qubits, necessitating the use of multiple qubits to represent a single variable.

In this context, solving the minor-embedding problem while minimizing the number of qubits in the embedding is crucial. Using more qubits increases the solution space and, given the noise in the processors and its random nature, it also raises the error rate. However, finding an embedding for any Ising model into any processor while minimizing the number of qubits is an NP-Hard problem.

Note that the minor-embedding problem in the context of quantum annealing will remain in that complexity class as long as QA processors do not possess all-to-all connectivity. This condition is likely to persist in the future because, due to the 2D nature of superconducting-based processors, it is extremely challenging to construct all-to-all hardware of non-small sizes [19].

Because of the complexity of the minor-embedding problem, heuristic methods have to be employed for its solving. In the literature, the standard algorithm to solve the minor-embedding problem is *Minorminer*. This method, proposed by Cai et al. in 2014 [20], uses a greedy approach that iteratively constructs the embedding while minimizing at each step the total number qubits used to represent each variable. The algorithm is studied in detail in Section 4. *Minorminer* is accessible in the D-Wave problem solving platform [12] as the standard to embed generic problems into the different available

processors. Besides *Minorminer*, D-Wave offers another minor-embedding method specific to embed fully connected problems, called *Clique Embedding* (CE, [21]). This algorithm gives an embedding in polynomial time for a fully connected instance of a given size.

In addition to the methods provided by D-Wave, various independent research teams have proposed alternative approaches, including the following:

- Researchers in [22] present Layout-Aware Embedding, which utilizes the “location information” of variables within a problem to guide mapping heuristics. This location information can either be an inherent characteristic of the problem or be calculated using graph theory node placement algorithms. Once an initial embedding is achieved through this method, the *Minorminer* algorithm is employed to optimize it.
- In [23], two algorithms are proposed to search for an initial embedding, which is subsequently taken as an initial solution by *Minorminer*. The first method, termed *Clique-Based Minorminer*, utilizes the *Clique embedding* method by D-Wave to trivially embed a subset of variables, leaving the remaining variables unassigned to qubits. The second one, named *Spring-Based Minorminer*, is analogous to the layout-aware embedding algorithm presented in [22]. In a nutshell, it employs a tuned Fruchterman-Reingold spring algorithm to calculate a layout for positioning the variables and interactions of the problem in a plane. This layout information is then used to assign variables to qubits and construct an initial embedding.
- The team behind [24] present *Probabilistic-Swap-Shift-Annealing*, which is a minor-embedding algorithm inspired by the principles of simulated annealing. It begins by generating an initial embedding and then iteratively modifies it through probabilistic decision-making to enhance the embedding over successive iterations.
- In [25], the authors introduce the idea of a virtual hardware layer, which consists of a precomputed embedding of a biclique graph into the hardware, making the user calculate embeddings to the biclique instead of to the topology graph. The idea behind this method is that they propose a heuristic algorithm to calculate embeddings of problems into the biclique virtual hardware based on the graph theoretic concept of odd cycle transversal decomposition, which is less costly than embedding instances directly to the hardware.
- In [26], the minor-embedding problem is reformulated and solved using Integer Programming tools.

Despite the interest in these alternative methods, none have consistently surpassed *Minorminer* in terms of embedding efficiency, minimizing the required number of qubits, and computational effectiveness to warrant a change in its standard status. As a result, *Minorminer* remains the benchmark in the field. This study focuses on this algorithm due its standard status. The objective of this work is twofold:

1. Reveal the critical influence that the minor-embedding problem has on the final performance of quantum annealing. This is, the correlation between the quality of the embedding (solution to the minor-embedding problem given by Minorminer) and the quality of the final solutions given by the quantum annealer. This publication contains an in-depth study of this influence with both theoretical and experimental results.
2. Upon recognizing the significance of embedding quality, this work presents a comprehensive study of the Minorminer algorithm. This investigation encompasses a thorough analysis of the algorithm, from its foundational principles and pseudocode to the experimental evaluation of its limitations, capabilities, and performance as a minor-embedding algorithm.

The rest of the paper is organized as follows: the subsequent section provides a comprehensive overview of the problem-solving process using quantum annealers. In Section 3, the minor-embedding problem is formally defined and thoroughly described. Following this, the Minorminer algorithm and its strategy are theoretically analyzed in detail. Section 5 presents the experimental results of the study. Firstly, it evaluates the relationship between the quality of the embedding and the quality of the final solution to the problem. Secondly, it provides an experimental assessment of Minorminer to measure its capabilities and performance. This paper finishes highlighting the main conclusions and further work in Section 6.

2. The quantum annealing process

Solving a combinatorial optimization problem with a quantum annealer that samples low energy solutions of programmable Hamiltonians is a process composed of different steps, which are represented in Figure 1:

1. *Reformulating the Combinatorial Optimization Problem as an Ising Model:* First, the problem must be modeled as an Ising model. This can be accomplished using various mathematical techniques if the problem involves non-binary discrete variables and/or constraints [14].
2. *Minor-embedding Problem:* Then the Ising model must be adapted to fit into the quantum annealing processor. These processors consist of qubits and couplers between pairs of qubits, which sample low-energy states of Hamiltonians represented by the following form:

$$\sum_{i \in V} h_i \sigma_z^{(i)} + \sum_{(i,j) \in E} J_{i,j} \sigma_z^{(i)} \sigma_z^{(j)} \quad (1)$$

where $\sigma_z^{(i)}$ is the Pauli z operator acting on qubit i , and V and E are the sets of qubits and couplers in the given processor, respectively. For each existing qubit $i \in V$, h_i is its bias, and for each existing coupler $(i, j) \in E$, $J_{i,j}$ is its weight. After each execution of the annealer, the

state of each qubit is measured, resulting in solutions to the following Ising model:

$$\sum_{i \in V} h_i s_i + \sum_{(i,j) \in E} J_{i,j} s_i s_j \quad (2)$$

where s_i are the variables taking values $+1$ or -1 for all $i \in V$.

QAs can be regarded as programmable Ising model solvers. However, their programmability is constrained by the characteristics of the processors. The values h_i and $J_{i,j}$ can only be adjusted within a certain range, and the sets V and E , which define the possible binary variables and their interactions, respectively, are dependent on the architecture of the processor.

By considering the set of qubits V as the node set and the set of couplers E as the edge set, the processor's architecture is represented by the *topology graph* $G = (V, E)$. The Ising model can also be represented by the *problem graph*, where the nodes correspond to the variables and the edges represent the non-zero quadratic terms that connect pairs of variables. Representing both the problem and the hardware as graphs is crucial because the Ising models that can be solved on these machines are those whose problem graphs are subgraphs of the processor's topology. However, due to connectivity limitations in hardware, it is highly unlikely that the problem graph of an Ising model for a real combinatorial optimization problem is naturally a subgraph of any current quantum annealer's topology.

In this context, addressing the minor-embedding problem is required, which is done by intelligently selecting qubits or sets of qubits to represent the variables of the Ising model. The latter case is occasionally necessary, as this approach allows for the representation of variables with higher connectivity than the degree of the topology graph, thereby enabling the representation of an exponentially large number of Ising models. The sets of qubits assigned to single variables are referred to as *chains*.

Remark that there is not a unique way of embedding a given problem graph into a given hardware graph, and it is crucial to find the one which employs the least amount of qubits possible. This is because an increase in the number of qubits expands the solution space that the annealer must explore, which, due to imperfections in current processors, leads to a degradation in solution quality.

Upon solving the minor-embedding problem, the original Ising model is transformed into the *embedded Ising model*. The graph of this new model is a minor of the hardware's topology graph, and penalties are introduced to promote that qubits forming chains attain the same value at the end of the anneal. The strength of these penalties can be adjusted by the user in the D-Wave paradigm using the *chain-strength* parameter, although a default value is automatically calculated. Additionally, variable biases and interaction weights are adjusted to promote that the

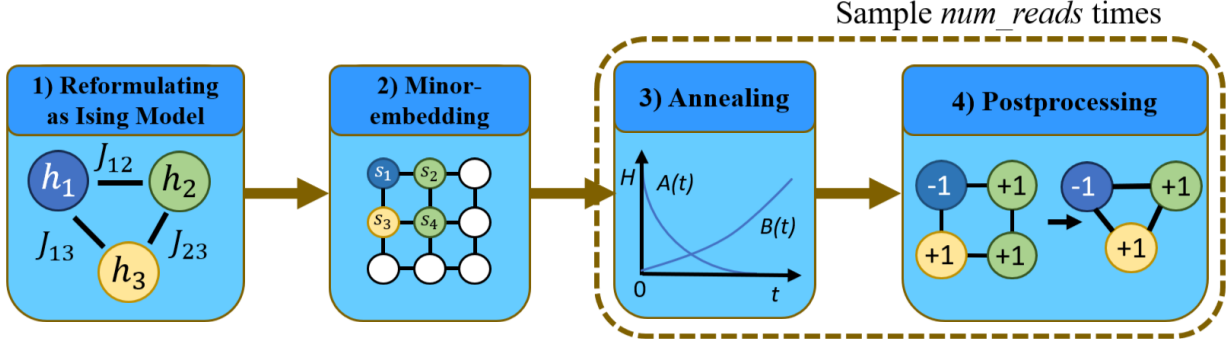


Figure 1: Flux diagram of the quantum annealing problem solving process in D-Wave Systems annealers. Inspired in [27], [28].

solution space encompasses that of the original problem. Consequently, the embedded Ising model can be solved via quantum annealing, and its solutions can be efficiently translated back to the original problem.

3. *Quantum Annealing*: This is the step executed by the quantum annealing processor. The quantum annealer is initialized in a physically easy-to-prepare state, and its Hamiltonian is gradually modified until it matches the problem's Hamiltonian in Equation (1), where the embedded Ising model is encoded. At the end of the evolution, each qubit's state is measured to obtain a solution to the embedded Ising model. Due to imperfections in current annealers and the probabilistic nature of the method, the annealer is run multiple times to generate a sample of solutions. The number of executions, referred to as *number of reads*, is determined by the user; however, it is recommended to perform at least 1000 executions [12].
4. *Postprocessing*: The sample must be postprocessed to get solutions to the Ising model. This process involves taking the final value of each qubit to determine the value of the corresponding Ising variable. When a variable is represented by a chain, two scenarios are possible: all qubits in the chain have taken the same value (i.e. there is a consensus), or qubits in the chain have differed in the readout of the sampling. The latter scenario is referred to as a *broken chain*. In D-Wave's quantum annealing paradigm, a broken chain is resolved through a majority vote among the qubits in the chain, assigning the winning value to the variable. Lastly, the solution to the Ising model is transformed to be of the form of the original combinatorial optimization problem.

Note that the quantum annealing approach described above is not applicable to problems of all sizes. When the Ising model exceeds a specific size and connectivity threshold, finding a minor-embedding into the topology graph becomes infeasible. In such cases, quantum annealing based hybrid computing methods, such as those offered by D-Wave [4], can be employed. However, this research area falls beyond the scope of this paper, as it involves additional classical methods beyond minor-embedding.

3. Minor-embedding problem

The minor-embedding problem emerged in the field of graph theory well before the advent of quantum computing. This problem has been examined in numerous publications, which explore its complexity and propose algorithms, such as those by Matoušek (1992) [29] and Robertson and Seymour (1995) [30] (the latter under the name of the minor containment problem). However, when applied to quantum annealing, the problem involves identifying the embedding that utilizes the minimum number of qubits, as mentioned in the previous section of this paper.

In this context, we formally define the minor-embedding problem using the following definition. We denote the node and edge sets of a graph G as $V(G)$ and $E(G)$, respectively, and the power set of a set A as $\mathcal{P}(A)$, which is the set of all subsets of A .

Definition 1

Given a pair of graphs, called source graph H and target graph G , the minor-embedding problem is the problem of finding the minimum minor of G that, by contraction of connected nodes, transforms into a graph isomorphic to H .

The solution to the minor-embedding problem is an *embedding* or *model*, which defines as a function $\phi : V(H) \rightarrow \mathcal{P}(V(G))$ subject to the following conditions:

1. **Vertex-model connectivity**: For every node $v \in V(H)$, $\phi(v) \subseteq V(G)$ forms a connected subgraph in G .
2. **Edge representation**: For every edge $(u, v) \in E(H)$, there exists one edge $(u', v') \in E(G)$ where $u' \in \phi(u)$ and $v' \in \phi(v)$.
3. **Vertex-model pairwise disjointness**: $\phi(u) \cap \phi(v) = \emptyset$ for all $u, v \in V(H)$ such that $u \neq v$. This is, every node in the target graph can only appear in the mapping of one source graph node.

The set $\phi(v)$ is called the *vertex-model* or *chain* of v .

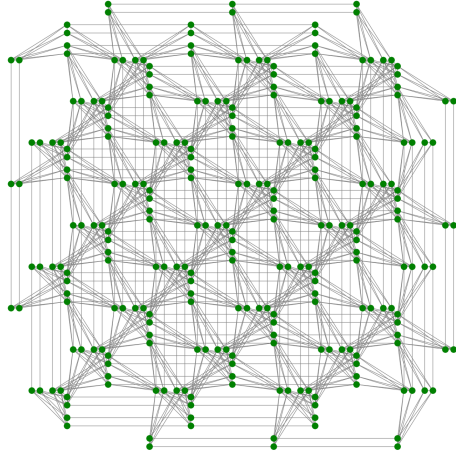


Figure 2: Section of a Pegasus graph. The size of the actual Pegasus employed in the processors follows the same shape but is 16 times larger in area. The graph has been generated with the D-Wave’s python library `dwave-networkx`, which is an extension of `Networkx` [33].

In the context of embedding Ising models into quantum annealers, the source graph represents the problem graph, while the target graph corresponds to the architecture of the quantum processor. The node set $V(H)$ in the source graph comprises the variables of the model, while the edge set $E(H)$ consists of pairs of variables that exhibit non-zero weighted quadratic interactions. Conversely, the target graph is defined with qubits as nodes and couplers as edges.

At the time of writing, the most advanced quantum annealers are D-Wave’s `Advantage_system` processors. These processors are constructed using a topology graph known as *Pegasus* [31], illustrated in Figure 2. This graph comprises 5760 nodes, with the majority having a degree of 15. In addition to the established `Advantage_system` processors, a prototype of the next-generation models is also available, which is called `Advantage2.prototype`. This new device features a higher connectivity topology known as *Zephyr* [32]. This new topology has a degree of 20 for the majority of the nodes. However, due to its early stage, this prototype is not as large as the established ones and features approximately 1200 qubits.

Although the ideal Pegasus graph is the one shown in Figure 2, in practice, certain qubits and couplers are excluded from the accessible programmable fabric due to operational malfunctions. The actual topology graph of an `Advantage_system` processor, which includes missing qubits or couplers, is referred to as a *broken* Pegasus graph, and the actual number of qubits of these graphs is around 5600. The number of couplers in the `Advantage_system` processors is approximately 40 000, resulting in a sparse graph with a density of

$$\frac{\text{existing couplers}}{\text{number of possible pairs of qubits}} \approx \frac{40\,000}{\binom{5600}{2}} \approx 0.0025.$$

This sparsity significantly limits the capabilities of these annealers.

Illustrative example

To illustrate the impact of the sparse density of quantum annealing processors, consider an example using the D-Wave `Advantage_system4.1`. Take an instance of the well-known Traveling Salesman Problem (TSP) with n cities. When formulated as an Ising model, it requires n^2 variables, resulting in a fully connected problem graph [14]. Embedding a complete graph into Pegasus, due to its limited connectivity, necessitates extensive chains, thereby requiring a large number of qubits. Consequently, only fully connected Ising models with fewer than 200 binary variables can be embedded, thereby limiting the TSP instance to fewer than $\sqrt{200} \approx 14$ cities.

To summarize, solving the minor-embedding problem optimally is crucial for the following reasons:

- The performance of the end-to-end quantum annealing paradigm is influenced by the quality of the embedding, as will be demonstrated in Section 5.2.
- The size and density of the problems the quantum annealer can address depend on the ability to embed problems using the minimum number of qubits.

However, the relevance of the problem is further underscored by its computational hardness:

Proposition 1

The minor-embedding problem is NP-hard.

Proof. The problem of just finding an embedding without minimizing the size of the minor (the amount of qubits) is NP-complete. This is because for any given target graph, the special case of taking as source a cycle graph with the same number of vertices as the target, corresponds exactly to the Hamiltonian Cycle problem, which is one of Karp’s 21 NP-complete problems [34]. Also, its solution is polynomially verifiable by checking that all three conditions of the definition are fulfilled.

However, the minor-embedding problem as defined here is NP-hard because it is at least as hard as the NP-complete model, but no polynomial algorithm is known to verify the optimality of a given solution in terms of used number of qubits. \square

It is important to note that the previous result is proven for the problem with source and target graphs as inputs. In the quantum annealing paradigm, this is not exactly the case because the target graph is not fully variant; it is restricted to slightly broken versions of specific topologies such as Pegasus, Zephyr, or other topology graphs of different quantum annealers. However, as demonstrated by Lobe and Lutz in [35], the variants with missing vertices and edges in these broken topology graphs maintain the problem within the same complexity class.

As a result of the problem’s complexity, heuristic methods must be employed, which have inherent disadvantages. These include suboptimal embeddings that introduce unnecessary noise and the inability to embed problems that could theoretically be embedded, further diminishing the quantum annealer’s capabilities. Moreover, finding the actual minor-embedding typically demands significant computational time. The classical solving of the minor-embedding problem can delay the quantum annealing process, potentially negating any speedup advantages.

4. Minor-embedding algorithm on D-Wave: Minorminer

This section presents a theoretical analysis of Minorminer, the established approach within the D-Wave quantum annealing framework for achieving this objective. For a more comprehensive understanding, readers are directed to the original work [20].

In a nutshell, the Minorminer takes as input a pair of source and target graphs and employs a greedy strategy to iteratively construct a solution to the minor-embedding problem. The objective is to construct an embedding ϕ as in Definition 1 that minimizes the number of qubits needed for the mapping.

The strategy involves initially constructing a preliminary solution and iteratively refining it to achieve better solution quality. However, the simpler problem of constructing a valid embedding to begin with, i.e., finding any (not necessarily minimal) embedding that satisfies all three conditions of Definition 1, is already NP-complete. Consequently, Minorminer relaxes the minor-embedding problem by focusing on fulfilling only the vertex-model connectivity and the edge representation conditions (1 and 2 in the definition), while incorporating a penalty term in the objective function for instances where the vertex-model pairwise disjointness condition (number 3) is not met. This approach enables the identification of an initial embedding in polynomial time, with the penalty term guiding the algorithm towards valid embeddings as the execution progresses. When condition 3 is not satisfied, the embedding is deemed invalid, and qubits representing more than one variable are referred to as *overlapped*.

Minorminer, akin to every other greedy algorithms, iteratively makes locally optimal decisions at each step to achieve a solution to the overall problem. Under these circumstances, the local choices involve optimally setting the vertex-model to satisfy conditions 1 and 2 for each variable, while:

- Minimizing the degree of the maximally overlapped qubit, i.e., the maximum number of vertex-models to which a single qubit is assigned. Additionally, minimizing the quantity of these maximally overlapped qubits.
- Minimizing the total number of qubits needed for the model.

The selection of the vertex model for each variable is managed by an auxiliary function, defined as *find_minimal_vertex_model*. This function employs a weighted minimum path search algorithm within the target graph to identify the qubit closest to all

the vertex-models of the variable’s neighbors, assigning additional weight to each used qubit as a penalty term. The vertex model is then constructed with that qubit and the ones forming the paths to the neighbors. In this context, the weight assigned to each qubit is the diameter of the target graph, defined as the largest possible distance between any two nodes, raised to the power of the number of vertex-models that include it:

$$w(g) = \text{diameter}(G)^{|\{v_i \in V(G) : g \in \phi(v_i)\}|} \quad (3)$$

where G is the target graph, $V(G)$ its set of nodes and ϕ is the embedding. The idea behind this weighting strategy is to guide the algorithm towards valid embeddings, even if it requires large chains, with the diameter of the target graph representing the largest possible qubit chain.

The core mechanism of Minorminer involves iteratively traversing through the source nodes, updating each vertex model at every step by considering the most recent versions of all other models. Upon completing a traversal of all variables, a *loop* is considered complete. The process of executing a loop is described in Algorithm 1.

Algorithm 1: execute_loop

Input: source graph H with ordered variables $\{v_1, v_2, \dots, v_n\}$, target graph G , embedding ϕ

Output: updated embedding ϕ

```

1 for  $v_i \in \{v_1, v_2, \dots, v_n\}$  do
2   for each qubit  $g \in V(G)$  do
3      $w(g) := \text{diameter}(G)^{|\{j \neq i : g \in \phi(v_j)\}|}$ 
4    $\phi(v_i) := \text{find\_minimal\_vertex\_model}(G, w, \{\phi(v_j) : v_j \sim v_i\})$ 
5 return updated embedding  $\phi$ 

```

The initial loop typically begins with an empty model and generates the first embedding, which is often invalid. The algorithm then performs numerous iterations, progressively minimizing the objective function until a valid embedding is found or the algorithm ceases to improve the objective function. Subsequently, Minorminer continues iterating with a modified objective function aimed at minimizing the total number of qubits.

Given that the objective function of the algorithm is defined differently during its execution, we propose conceptually dividing the algorithm into two distinct phases. Although the authors of the original paper present a simpler version without this distinction, we find it more intuitive to separate the algorithm into two phases. The first phase, called *valid embedding-finding phase*, aims to find a valid embedding. The second phase, called *chain shortening phase*, commences once a valid embedding has been found and focuses on shortening the chains of the embedding.

The two phases are discussed in more detail below, providing the detailed information behind Algorithm 2:

- *Valid Embedding-Finding Phase* (lines 1-7): Minorminer begins by randomly determining the sequence in which the vertex models will be computed. As the algorithm is generally initialized with an invalid embedding (empty by default), this phase involves repetitively executing loops to

minimize the degree and number of maximally overlapped qubits until the embedding becomes valid. The objective function in this phase is defined as follows:

$$\min_{\phi} \left(\max_{g \in V(G)} |\{v_i \in V(H) : g \in \phi(v_i)\}|, \right. \\ \left. \text{number of } g \text{ in that condition} \right) \quad (4)$$

where the parentheses denote a lexicographic optimization approach, $V(G)$ is the target graph node set and ϕ the embedding.

Upon achieving a valid embedding, the algorithm transitions directly to the second phase. However, due to the greedy nature of the method, it can sometimes get stuck in local minima corresponding to invalid embeddings. To mitigate this, the algorithm is interrupted if there is no improvement in the objective function over a specified number of loops, which is set to 10 by default. The parameter to specify this number of failed loops is referred to as *max-no-improvement*. In such cases, the algorithm restarts from the beginning, marking the completion of a *try*. By default, Minorminer performs up to 10 tries before ceasing attempts to solve the problem and returning a failure message, but this value can be adjusted with the *tries* parameter.

- *Chain Shortening Phase* (lines 8-12): The objective of this phase is to minimize the total number of qubits in the embedding. Formally, the objective function is defined as

$$\min_{\phi} \sum_{v_i \in V(H)} |\phi(v_i)| \quad (5)$$

where $V(H)$ is the source graph node set and ϕ the embedding.

The process is procedurally similar to the previous phase, with the stopping criterion based on a specified number of loops without improvement. The *chain-length-patience* parameter adjusts this patience number, which is set to a default value of 10. Once this condition is met, the best-found embedding is returned.

Note that the algorithm executes the second phase only once, greedily shortening the chains of the first found valid embedding without ever comparing it to others from different initializations. This purely greedy strategy limits exploratory capabilities, as shown in the final section of this study. However, more exploratory methods could significantly increase run times, potentially making the quantum annealing method impractical.

Finally, Minorminer incorporates a *timeout* feature as its ultimate stopping criterion, interrupting the process if it exceeds a specified duration. If this occurs during phase two, the best embedding found is returned. If it happens during phase one, an empty embedding is returned, indicating no valid embedding has been found. The default timeout is 1000 seconds.

Algorithm 2: find_embedding

Input: source graph H , target graph G

Parameters: max-no-improvement, chain-length-patience, tries

Output: embedding ϕ or fail message

```

1 Define the objective function
   $f(\phi) := (\max_{g \in V(G)} |\{v_i \in V(H) : g \in \phi(v_i)\}|, \text{number of } g \text{ in that condition});$ 
2 for try in tries do // Here starts phase 1
3   Randomize the source vertex order  $\{v_1, v_2, \dots, v_n\}$ ;
4   while  $f(\phi) > 1$  and  $f(\phi)$  improved in the last
     chain-length-patience loops do
5      $\phi = \text{execute\_loop}(H, G, \phi);$ 
6   if  $f(\phi) > 1$  then // Phase 1 failed to find a
     valid embedding
7     Start new try
8   else if  $f(\phi) = 1$  then // Here starts phase 2
9     Redefine the objective function  $f(\phi) := \sum_{v_i \in V(H)} |\phi(v_i)|;$ 
10    while  $f(\phi)$  improved in the last chain-length-patience
       loops do
11       $\phi = \text{execute\_loop}(H, G, \phi);$ 
12    return  $\phi$ 
13 return no valid embedding has been found
```

5. Experimentation

Given the comprehensive background provided on the minor-embedding problem in quantum annealing, we now present the core findings of this study. This section aims to experimentally address the following closely interrelated research questions (RQs).

RQ1: *What is the impact of the embedding quality on the performance of the quantum annealer?* (Section 5.2)

QA's performance is influenced by different factors such as noise in the processors and the nature of the energy landscape of the Ising model. In this context, we hypothesize that the error in quantum annealing is exponentially correlated with the number of qubits used in the embedding.

Noise is naturally unpredictable, and the energy landscape can only be assessed once the problem is analytically solved, making preemptive adjustments unfeasible. However, the number of qubits in the embedding is known prior to sending the problem to the processor. Thus, although not a holistic performance predictor, our hypothesis offers insights into the annealer's problem-solving efficacy based on the embedded problem's size.

RQ2: *How good is Minorminer as a minor-embedding algorithm for quantum annealing?* (Section 5.3)

Given that Minorminer is the standard method for embedding problems into D-Wave's annealers, evaluating its performance

is crucial. This analysis provides insights about the expected quality of embeddings of a given problem. When combined with the previous point, it helps predict the anticipated performance of the end-to-end quantum annealing solution.

Section 5.1 will provide the detailed configuration of the experiments to ensure the reproducibility of the results.

5.1. Experimental setup

Three experiments were conducted in this study: two addressing RQ1 and one addressing RQ2.

Instance generation. The problems to be solved along the whole experimentation are Ising models which have been generated following a two-step procedure:

- Initially, the problem graph is randomly constructed using the Erdős-Rényi (ER) algorithm [36], tailored to specific problem sizes and densities. The algorithm has been selected because, due its uniformly random nature, it is the most general and unbiased at emulating the set of all possible graphs with a given number of nodes and edge probability (density).
- Subsequently, random numerical values are assigned to the variable biases at the nodes and the interaction strengths at the edges. These values are uniformly selected from the range $[-1, +1] \subset \mathbb{R}$ to prevent degenerate instances.

Note that for the RQ2 experiments, which focus exclusively on embedding instances, generating the graph is sufficient, leaving aside the subsequent resolution of the problem.

Infrastructure. All Ising models were solved using the D-Wave Advantage_system4.1 processor, which, at the time of writing, is the largest model available (the one with least amount of broken qubits), featuring 5627 qubits arranged in a broken Pegasus topology. The processor has been operated with default parameters, and the number of reads per annealing process has been set to 1000 reads.

Minorminer has been executed differently for each of the two research questions:

- For RQ1, the chain-length-patience parameter has been set differently trough the different executions (see Table 1), which results in a higher variance in embedding ACL values. This setup has been chosen to obtain a broader and more varied sample, allowing for the observation of the exponential relationship between QA performance and embedding ACL.
- For RQ2, the chain-length-patience parameter has been set to its default value (10), as the goal has been to assess the algorithm’s capacity.

After finding each embedding, the chain-strength parameter has been set default in all of the cases. Furthermore, the size, density, and number of problems generated and solved varied across the experiments, as did the number of embeddings per problem and Minorminer’s chain-length-patience parameter. This information is detailed in Table 1.

Evaluation procedure. As D-Wave quantum annealers work as sampling machines, it is more pertinent to consider the median energy of the sample rather than the solution with the minimum energy to accurately assess the machine’s performance. While the best-found solution is obviously more interesting when solving a problem, the median is arguably more representative of the entire sample. Therefore, the results presented in this study are based on the median value of the sample of results.

Furthermore, since the annealer tackles the embedded problem, it is more pertinent to evaluate the solutions to the embedded problem (after step 3 in Figure 1) rather than the postprocessed ones (after step 4 in Figure 1), which can be altered by classical methods. Nevertheless, as the energies of both the solutions to the embedded problem and the postprocessed solutions exhibit values within the same range of values, these values can be shown side by side. Therefore, in Section 5.2 both sets of solutions are studied.

Metrics. Regarding the metrics employed to asses the quality of the results, on the one hand, the solutions provided by the QPU are measured using the relative error. This metric quantifies the ratio of the deviation of the energy of the solution with respect to the energy of a reference solution. The reference solutions used along the experimentation have been taken as the best from the two provided by the D-Wave implemented versions of the following classical algorithms: MST2 multistart tabu search algorithm [37] and simulated annealing sampler [38]. Thus, the relative error is calculated as follows:

$$e_{rel} = \left| \frac{energy_{ref} - energy_{QA}}{energy_{ref}} \right|$$

where $energy_{ref}$ is the energy of the solution found by the reference solver and $energy_{QA}$ is the energy of a solution given by the annealer, i.e., the energy of an outcome after step 3 in Figure 1.

On the other hand, the quality of an embedding can be evaluated using two different but related metrics. The first one is the total number of qubits needed in the embedding, i.e.,

$$n_{qubits} = \sum_{v_i \in V(H)} |\phi(v_i)|,$$

and the second one is the *average chain length (ACL)*, defined as follows:

$$ACL = \frac{n_{qubits}}{size(model)}$$

where $size(model)$ is the number of variables in the original Ising model. As the size of the Ising models varies throughout the experiments, we have chosen to use the latter metric because it is normalized by the number of qubits, making it more representative for comparing embeddings of Ising models with different sizes.

The comparison between QA performance and embedding quality is therefore quantified by the median relative error of the embedded problem solution sample, relative to the ACL of the embedding used to solve the problem.

Experiment	Sizes	Densities	Problems ⁴	Embeddings ⁵	CLP ⁶
RQ1.1	{25, 45, ..., 175}	{0.05, 0.1, ..., 1}	5	10	{0, 1, ..., 10}
RQ1.2	150	0.5	5	100	{0, 1, ..., 10}
RQ2	{10, 15, ..., 300}	{0.05, 0.1, ..., 1}	1	64	10

⁴ Number of problems per density and size.

⁵ Number of embeddings per problem.

⁶ CLP stands for Minorminer’s chain-length-patience parameter.

Table 1: Experimental setup for the three experiments.

5.2. RQ1: What is the impact of the embedding quality on the performance of the quantum annealer

In general, problems with larger solution spaces are more challenging to solve than those with smaller ones. As previously discussed, optimal embeddings minimize the number of qubits used, while poor embeddings result in larger embedded problems. Even when the embedded problem is correctly modeled, an increase in its size expands the solution space within which the quantum annealer operates, thereby reducing the probability of obtaining high-quality solutions. The growth of the solution space is analytically measured in the following proposition:

Proposition 2

Let have an Ising model with $n \in \mathbb{N}$ variables. Let have two different embeddings for the instance onto a hardware topology graph with average chain lengths ACL_1 and ACL_2 , and define the solution spaces of their embedded Ising models as S_1 and S_2 , respectively. Assume $ACL_1 < ACL_2$. The ratio between the sizes of the solution spaces is given by:

$$\frac{|S_2|}{|S_1|} = 2^{n(ACL_2 - ACL_1)}.$$

Proof. For any binary unconstrained model such as Ising model or QUBO, when embedded into a certain topology graph, the size of the solution space of its embedded version S is $|S| = 2^{n_{qubits}} = 2^{n \cdot ACL}$. \square

D-Wave’s quantum annealers sample from a problem-specific energy-based distribution function [12], which is altered by noise [39] [40] [41]. This probabilistic behavior, combined with the exponential growth in the solution space, suggests an exponential increase in the error of the annealer as the ACL of the embedding increases. In the following, this result is experimentally studied.

Having said that, two experiments have been carried out to investigate the nature of the relation between the quality of the embedding and the quality of the solution to the embedded Ising model.

RQ1.1: Embedding Impact - General Case. The first experiment measures the relationship between embedding quality and QA performance for a set of 400 Ising models with varying

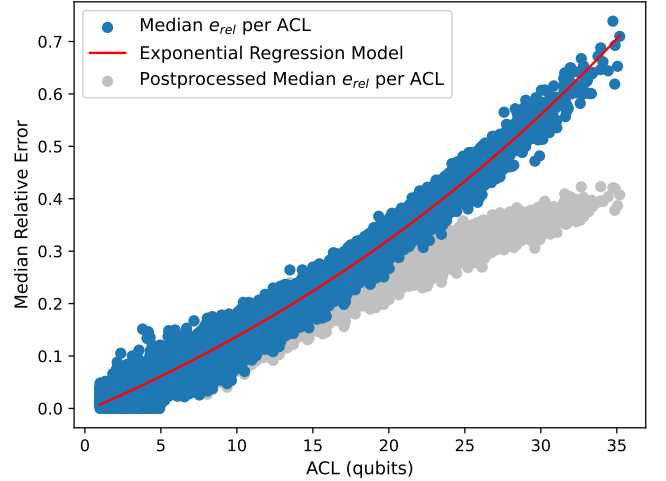


Figure 3: The blue dots represent the median relative errors over the ACL of the embeddings used for each solution sample. These samples are derived from solving randomly generated Ising models as described in Table 1. The red line illustrates an exponential ACL-relative error regression model. The silver dots represent the median relative errors of the postprocessed solutions.

sizes and densities across the entire embeddable range (detailed in Section 5.3). The aim is to assess this relationship across different scenarios and empirically test its exponential nature over a wide range of problems. The results are represented in Figure 3.

A cursory examination of the blue dots in the figure reveals a stringent correlation between the two variables, depicted by a consistent curve. To numerically analyze the nature of this curve, an exponential regression model has been applied to the dataset obtained from the experiment, which is illustrated by the red line. The fitting has been executed using the least squares method, achieving an r-squared value of 0.981. The high r-squared value underscores the significance of the exponential regression and corroborates our hypothesis. This robust conclusion emphasizes the critical importance of effectively addressing the minor-embedding problem.

The silver dots represent the median relative errors of the postprocessed solutions. While the errors for the postprocessed solutions exhibit an increase, this increase is less pronounced compared to the solutions returned by the annealer. Nonetheless, there is a clear positive correlation between the ACL and the median relative error of postprocessed solutions. It is evi-

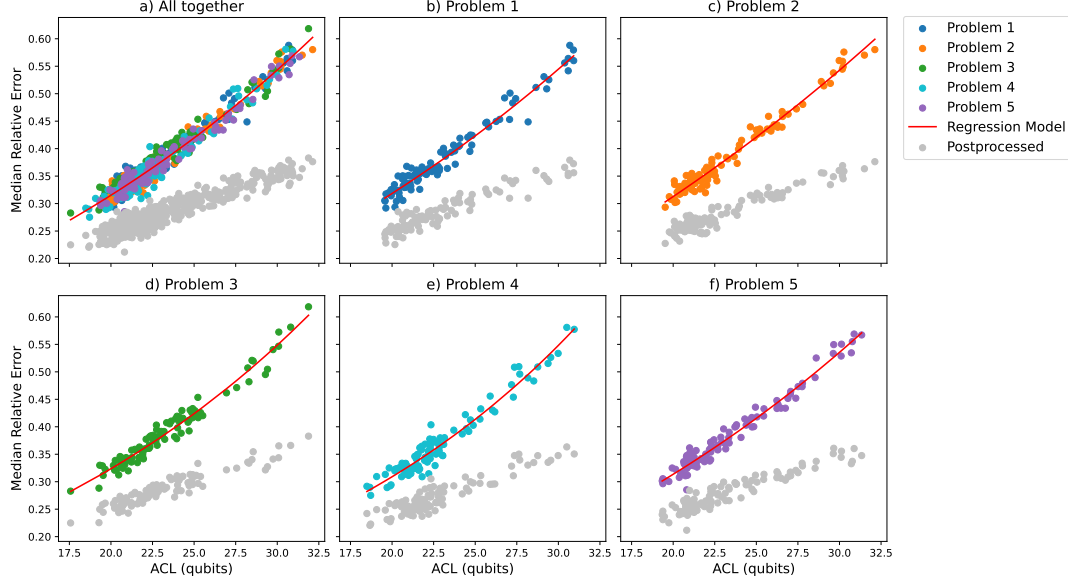


Figure 4: (a) Median relative errors of 100 solution samples for 5 random problems (see Table 1) over the ACL of their embeddings. A different color has been given to the outcome of each problem. The red line represents the exponential regression model fitted for all the dots. The silver dots correspond to the median relative errors of the same solutions after the postprocessing. (b-f) Same scatter plot for each random problem, with the fitted exponential regression models for each problem as red lines. Silver dots are postprocessed solutions.

dent that a larger search space leads to poorer solutions for the embedded Ising models, and consequently, to inferior postprocessed solutions for the Ising model being solved.

RQ1.2: Embedding Impact - Stressed. The second experiment also measures the relationship between the QA performance and the embedding quality, but with a fixed problem density and size. In this scenario, the variance in QA performance is primarily influenced by the ACL, as the embedding is the sole variable for each generated problem during the executions. The fixed density and size values were chosen to be close to the embeddable limit (explained in more detail in 5.3) with the intention of being representative of non-trivial problems and stressing Minorminer to produce worse embeddings. The results, presented in Figure 4, illustrate the median relative errors of 100 solution samples for 5 different problems, as detailed in Table 1, plotted against the ACL values of their embeddings.

Given the fixed problem size and density, the variance in the number of qubits is lower than in the first experiment, and therefore the exponential trend is not as clearly observed. Nevertheless, as with the previous experiment data, in this case five exponential regression models have been fitted for each one of the problem’s outcomes. All the exponential regression models for each of the problems have been fitted with a r-square value of around 0.95, confirming once more the hypothesis.

The silver dots represent the median relative errors of the postprocessed solutions. As in the previous experiment, the increase in error for the solutions to the embedded Ising models also results in an increase in the postprocessed solutions. It has been empirically shown once again that an increased embedding ACL results in inferior solution quality for the embedded Ising models, which subsequently leads to inferior postprocessed solutions for the original Ising model.

Summary RQ1

A higher ACL in embeddings results in exponentially larger solution spaces for embedded Ising models, which translates to exponentially worse sampled solutions by the quantum annealer. Addressing RQ1 empirically demonstrates that the performance of the end-to-end quantum annealing technique significantly correlates negatively with the average chain length of the embedding employed to solve the Ising model.

5.3. RQ2: How good is Minorminer as a minor-embedding algorithm for quantum annealing?

To evaluate the performance and capabilities of Minorminer as a minor-embedding algorithm, this section will examine three key aspects:

- the ability to obtain valid embeddings,
- the quality of these embeddings,
- and the dispersion of the quality of embeddings.

All three aspects have been studied based on the results of an experiment that involves repeatedly executing Minorminer to embed different problem graphs as specified in Table 1. In addition, Clique Embedding has been utilized to solve the same problems, serving as a baseline for comparison with Minorminer’s performance. Clique Embedding identifies embeddings for fully connected graphs of a specified size within a target graph. These embeddings can then be applied to graphs of any connectivity with the same number of nodes, making CE

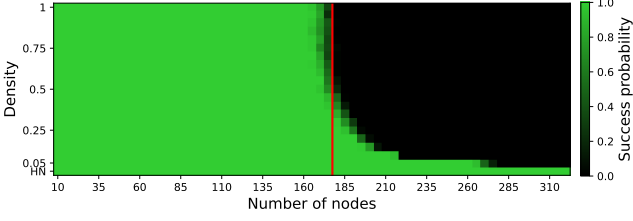


Figure 5: Probability of success of Minorminer finding a valid embedding for ER graphs into D-Wave Advantage_system4.1's broken Pegasus, as a function of density and size of problem graph. The red line represents the embeddable limit for CE. HN corresponds to Hardware Native instances, taken as the lowest significant density value.

useful as a worst-case scenario in terms of qubit usage (ACL). This algorithm is preprocessed once for the given target graph and subsequently generates embeddings in a deterministic way for a given size of complete graphs in polynomial time, which is significantly faster than Minorminer. The size of the maximum embeddable complete graph is contingent upon the topology graph. For the D-Wave Advantage_system4.1 processor's broken Pegasus, this value is 177 nodes. The ACL of these embeddings is always the same for a given complete graph size, which increases linearly with the number of nodes in the instances.

Embeddability boundary. The primary objective is to delineate the boundary between instance graphs that can be embedded into D-Wave's processor topology graphs and those that cannot. Although this boundary is inherently a property of the topology graph, it is also affected by the limitations of the heuristic algorithm employed for the embeddings. Due to the intractable nature of the problem, it is not feasible to determine this boundary precisely. Consequently, in practical terms, this boundary can be considered a characteristic of the heuristic method employed. As the results are inherently variable, the boundary is measured by the probability of obtaining a valid embedding.

Figure 5 illustrates the probability of Minorminer of finding a valid embedding as a function of the problem graph's density and size. This probability has been determined by counting the number of valid embeddings found across 64 executions per graph. The lowest density value of the figure corresponds to hardware native graphs, which are trivially embeddable for sizes up to 5600.

The results highlight the significant constraints in solving non-sparse instances using D-Wave quantum annealers. The insights drawn from the example in Section 3 are confirmed: the combination of the hardware's limited connectivity, the complexity of the minor-embedding problem, and the heuristic nature of Minorminer severely restricts the size of non-sparse embeddable instances. The following are the key observations to be made from Figure 5:

- Despite the hardware containing over 5600 qubits, the size of ER graphs with a density of 0.05 is limited to approximately 275. When the density exceeds 0.5, this value decreases to 175.

- Also, note that the boundary between embeddable and non-embeddable graphs is not a simple linear function of the problem's size or density. The size of the largest embeddable instances decreases rapidly at lower density values, but this decline becomes less pronounced as the density increases. In fact, the curve becomes almost vertical, suggesting that the maximum embeddable instances for fully connected graphs and those with a 0.5 density are of the same size, even though the latter possesses only half the interactions of the former.

A possible explanation to this phenomenon is attributed to the constraints imposed by embedding graphs that are significantly denser than the topology graph. For density values exceeding 0.5 and graph sizes greater than 160 nodes, the average degree of the Ising models surpasses 80 interactions per variable, which is more than five times the degree of the qubits in the hardware. Consequently, the algorithm addresses this by constructing qubit chains that are so extensive that it is probable that every pair of variable chains intersects at some point within the hardware graph. As a result, beyond a certain density value, it becomes equally challenging to embed problems of any density. This phenomenon is examined in greater detail by analyzing the ACL of the valid embeddings, as illustrated in Figure 6.

- The last observation pertains to the comparison between Minorminer's boundary and that of CE, represented by the red line. For sizes approaching 175 and densities greater than 0.5, Minorminer does not consistently find valid embeddings, unlike CE. This outcome is expected for complete graphs or density values near 1, where CE is typically recommended due to its deterministic nature. However, Minorminer remains inconsistent for lower density values, making CE a more reliable candidate for densities down to 0.5. When the density falls below this threshold, Minorminer begins to outperform CE in finding valid embeddings, with its performance improving as the instances become sparser, as anticipated.

Embedding quality. As have been seen in RQ1, the quality in ACL of embeddings has a critical influence in the performance of quantum annealing. Also, the ability to embed larger and denser instances is heavily dependent on constructing embeddings with the lowest possible ACL values. In Figure 6, we examine the ACL of Minorminer-constructed embeddings across various ER graphs of different sizes and densities. This analysis aims to explore the dependence of ACL on these two variables, thereby enhancing our understanding of the embeddability boundary curve. The following are the main observations from this figure:

- Panel (a) in Figure 6 illustrates the average ACL derived from 64 embeddings for each problem size and density values, considering only valid embeddings. The following trend can be observed in this figure: for densities below 0.5 the ACL rapidly increases with the density, but

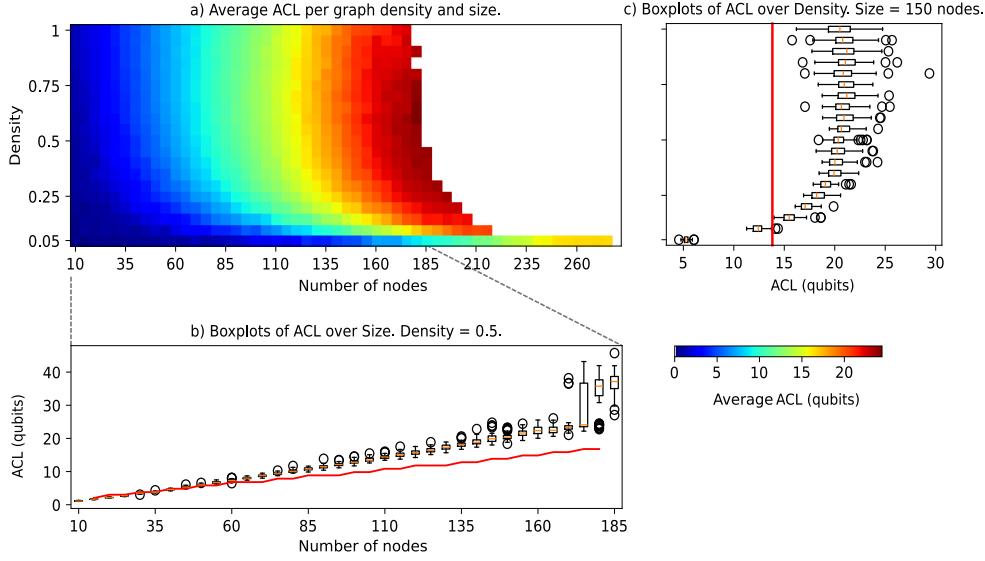


Figure 6: (a) Average ACL of valid embeddings from 64 ER graphs, per size and density. (b) Boxplots of ACL values of the 64 embeddings of the given size, for graph density fixed to 0.5. Red line represents the ACL of the CE embeddings. (c) Boxplots of ACL values of the 64 embeddings of the given density, for graph size fixed to 150. Red line represents the ACL of the CE embeddings.

for densities greater than this value, the average ACL does not appear to vary with density and correlates solely with the size of the instances. Conversely, for densities below this value, there is a curve similar to that observed at the embedding boundary. In the sparsest instances, the ACL decreases rapidly as the density decreases. This phenomena is deeper studied in the observations of panel (c).

- Panel (b) features problem graphs with a fixed density of 0.5. Instead of displaying the average ACL, this panel presents boxplots that show the complete data distribution. This density value has been chosen to avoid bias towards either sparse or highly connected graphs. The boxplots in the figure exhibit a linear growth with problem size, similar to the linear growth presented by Clique Embedding, represented by the red line. Notably, when the size of the instances surpasses 60 nodes, the red line falls below the boxplots, indicating that CE has returned embeddings using a smaller number of qubits. Given that these 0.5 density instances are far from being completely connected—the specific scenario in which CE is expected to outperform Minorminer in terms of qubit usage—this suggests that Minorminer performs worse than anticipated.

Moreover, as the size of the Ising models approaches the embeddable limit, the heuristic nature of the algorithm leads to increased instability, which is reflected in the suddenly wide range of the last boxplots. This instability results in a higher probability of Minorminer returning sub-optimal embeddings. The stability of these results is examined in greater detail later in Figure 8.

- Panel (c) displays boxplots of the ACL for embeddings identified in problem graphs with a fixed size of 150 nodes. This size has been selected to be close to Minorminer's

embeddability boundary observed in Figure 5. Three key observations can be made solely from this panel.

- The first observation to be made is the low density value at which the boxplots (Minorminer's embeddings) present a higher ACL than the red line (CE's), revealing a strong limitation in Minorminer's ability to minimize qubit usage in embeddings. This happens between the density values 0.10 and 0.15, once again, significantly far of being close in density to completely connected graphs. More precisely, between 0.10 and 0.15 is the region in which the instance graphs surpasses the hardware topology graph in average degree (average number of edges per node). This observation provides insight into characterizing the Ising models that present challenges so difficult for Minorminer that it falls behind CE in embedding quality. A more general comparison between the qualities of Minorminer's and CE's embeddings is illustrated in Figure 7, where the relationship between this comparison and the average degree of the instances is examined in greater detail.
- The second observation is that as the graph density increases, the median ACL values initially rise; however, the curve plateaus once the density surpasses 0.4. This phenomenon is strongly related to the flattening of the embeddability boundary shown in Figure 5. As mentioned in the observations of that figure, a possible explanation for this phenomenon lies in the challenges of embedding graphs with average degrees significantly higher than the average degree of the qubits in the hardware. Specifically, instances with 150 nodes and a density of 0.4 present an average degree of 60, which is four times that of Pegasus.

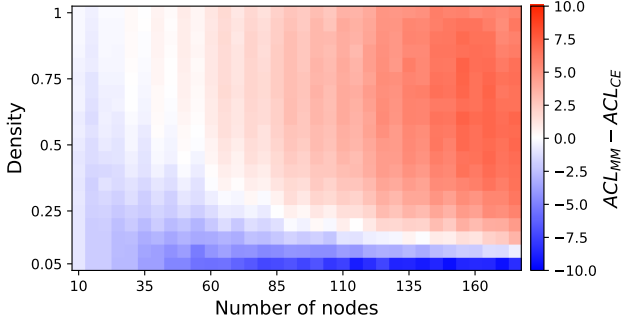


Figure 7: Difference in ACL between Minorminer’s and CE’s embeddings. The blue region corresponds to instances where Minorminer achieves better ACLs, while the red region indicates where CE performs better.

Minorminer struggles with such embeddings, resulting in a network of extensive chains of around 20 qubits. Given that Pegasus has a diameter of 33—the maximum distance between any pair of nodes—it is likely that every pair of variable chains intersects at some point within the hardware graph. Consequently, with a similar number of qubits, it becomes feasible to embed even a fully connected graph by simply activating every coupler at those chain intersections. Note that this explanation should be further investigated in future work; however, this task is challenging because the minor-embedding problem is computationally intractable for these instances, and therefore Minorminer’s results cannot be compared with the optimal embeddings.

- The third observation has to do with the range of the boxplots as the density increases. The range expands rapidly, indicating a high dispersion within the recorded ACL values for each density. For instance, in the 150-node instances, at a density of 0.7, the ACL values span from approximately 19 to 24, resulting on embedded Ising models of sizes spanning from 2850 to 3600 qubits. This substantial variation can lead to significantly poorer QA performance, as discussed in RQ1 (Section 5.2). Additionally, the increasing range of the boxplots with density, combined with the flattening of their median values, suggests that there is potentially a higher likelihood of obtaining a better ACL valued embedding when calculating embeddings for fully connected instances compared to those with a density of 0.5. However, this preliminary observation warrants further in-depth study.

As a part of the study of the quality of Minorminer’s embeddings, motivated by the unexpectedly wide range of Ising models in which CE happens to outperform it, a broader comparison between embeddings ACLs of the two methods has been conducted. This comparison is presented in Figure 7, which illustrates the mean difference in ACL between the two methods for each size and density value.

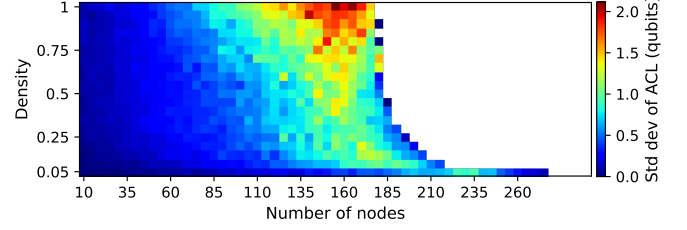


Figure 8: Standard deviation of ACLs calculated from the valid embeddings obtained during the 64 executions of Minorminer per size and density.

It is anticipated that CE would excel in problems with high connectivity, as indicated by the flattening of the curve in Figure 6c, which suggests excessive qubit usage for non-sparse instance embeddings. However, as the problem size increases, CE outperforms Minorminer in instances with a density lower than 0.25. Upon examining the region where CE yields superior embeddings, it has been observed that this occurs precisely in instances where the average degree of the source graph surpasses that of the topology graph. This observation is intuitively reasonable due to the high complexity of the minor-embedding problem, particularly in cases where the source graph is more connected per node than the target graph. In such scenarios, the problem becomes critically challenging for a greedy search algorithm like Minorminer. In this experiment, the topology graph used has been a broken Pegasus. However, the same phenomenon has also been observed in a preliminary experiment with the new Zephyr topology of D-Wave Advantage2.prototype. These preliminary results warrants further in-depth study.

Performance dispersion. The final measurement of Minorminer’s performance in the experiment involves stability of the algorithm’s embeddings quality. Figure 8 illustrates the standard deviation of ACLs for the 64 calculated embeddings per size and density, thereby showing the algorithm’s performance stability.

Minorminer exhibits high stability in small instances, indicated by a standard deviation lower than 0.5 qubits; and a notable stability in low-density larger ones, with this value slightly higher at around 1 qubit per chain. However, as instance size and density increase, the standard deviation significantly grows, reaching up to 2 qubits per chain. This variability implies that Minorminer can produce embeddings with differences in ACL of up to 4 qubits per chain for the same problem. Consequently, this not only results on a reduced likelihood of achieving the optimal embedding in a single run, but also on a significant probability of obtaining a notably bad embedding. Note that in the vicinity of the embeddableness boundary, the standard deviation decreases suddenly. This phenomenon occurs because the study only considers valid embeddings. Consequently, this reduction does not imply that the algorithm is stable; rather, it reflects the limited number of valid embeddings available for calculation.

The substantial dispersion in Minorminer’s embedding ACL values is particularly concerning within the quantum anneal-

ing framework of D-Wave, where the algorithm is typically executed only once to expedite the overall process. Therefore, there is a considerable likelihood that the embedded Ising model will be significantly larger than necessary, resulting in an exponentially larger solution space for the quantum annealer. This, in turn, leads to a higher error rate in the end-to-end quantum annealing method, contingent upon Minorminer’s stochastic behavior.

Summary RQ2

Minorminer, the default algorithm employed to minor-embed generic Ising models into D-Wave’s quantum annealers, exhibits worse performance than CE, which is expected to be the worst-case scenario for embedding algorithms in terms of qubit usage for non-complete Ising models. The following conclusions can be drawn from the experiment conducted in this section, focusing on the three key aspects mentioned earlier:

- In respect to the embeddableness boundary, Minorminer does not outperform CE in terms of the probability of finding embeddings for instances with densities ranging from 0.5 to 1.
- Regarding the embedding quality, Minorminer identifies embeddings with lower average ACL values compared to CE only for Ising model instances whose average degree is less than that of the topology graph. For the Pegasus topology studied, this value is 15 couplers per qubit.
- Lastly, Minorminer exhibits significant variability in the quality of embeddings for non-small and non-sparse Ising models. This is particularly notable when compared to CE, which is deterministic.

The combination of these three key aspects suggests that when the size of an Ising model is in the embeddable range of CE, this algorithm should be used to embed not only fully connected problems but also those with moderate connectivity due to its superior results, result stability, and polynomial time complexity.

6. Final Remarks and Future Directions

Despite significant advancements in the connectivity of quantum annealing processors, the realization of fully connected topology hardware on superconducting-based quantum annealers remains impractical due to their inherently two-dimensional architecture. Furthermore, optimizing quantum annealing performance necessitates addressing the minor-embedding problem with maximal efficiency, particularly concerning the required amount of qubits. Consequently, the minor-embedding problem is likely to persist as a substantial challenge in the future.

As a result of the conducted experiments, our investigation has identified the following answers to the research questions posed:

- RQ1: The minor embedding problem has a critical impact on the performance of the end-to-end quantum annealing paradigm. This is evidenced by the clear correlation between the average chain length of embeddings and the relative errors of the solutions sampled with those embeddings.
- RQ2: The default minor-embedding algorithm, Minorminer, has significant room for improvement. Clique Embedding outperforms Minorminer in terms of embedding quality, result stability, and time complexity across a significantly large set of non-sparse and non-small instances, where CE should be taken as the worse-case scenario. This set is larger than just the fully connected or nearly fully connected instances, which are theoretically the problems for which CE was created and is recommended to be used. Specifically, CE has outperformed Minorminer in embedding quality for all Ising models of size embeddable by CE (up to 177 nodes) with an average degree higher than that of the topology graph.

Based on the conclusions of this study, we propose the following strategy for solving generic Ising models (or QUBOs): If the problem falls within the embeddable range for both Minorminer and Clique Embedding, evaluate the average degree of the problem’s graph and compare it with that of the topology graph to determine the optimal embedding method. In scenarios where the average degree of the problem’s graph significantly exceeds that of the topology graph, the use of CE may be preferable over Minorminer. This perspective is novel, and we expect it to perform better than using Minorminer as the default in every non-fully-connected instance. Implementing this or other strategies to minimize qubit usage in embeddings is essential for fully leveraging the capacity of quantum annealers.

For future research, two primary directions are proposed, as illustrated in Figure 9. The first direction involves extending the experimental framework to further substantiate the conclusions drawn from this study. For instance, the relationship between the difference in ACL of embeddings generated with Minorminer and CE with the average degree of the problem, explained when examining Figure 7, should be studied more exhaustively for a larger set of target graphs. Additionally, the behavior of Minorminer’s performance in relation to the characteristics of the given source and target graphs (such as the flattening of the curve or the increasing dispersion) should be studied in greater depth. This would provide more robust answers to phenomena such as the flattening of the embeddableness boundary and the behavior of ACL with increasing instance size and density explained in Section 5.3.

To strengthen the conclusions of this study, although the Erdős-Rényi algorithm generates a wide range of varied graphs, the study could be expanded to include new graphs generated with different algorithms, such as Barabási-Albert [42] as in [23]. Additionally, this study could be repeated for any new

Extend the experimentation to:

- Other benchmarking graphs
- Other quantum annealers
- Other embedding algorithms
- Compare other aspects of embedding algorithms, such as execution time
- Analyze the relation between Minorminer and Clique Embedding performance for other problem and topology graphs

Ideas for future embedding methods:

- Utilizing a combination of CE and Minorminer to embed problems
- Enhancing solution quality through multiple executions (potentially parallel) of Minorminer
- Modifying Minorminer to a problem-aware algorithm

Figure 9: Two directions of future work.

quantum annealer relevant to the literature, whether it is a new model from D-Wave, such as the Advantage2, or from a different manufacturer. Furthermore, the experiments should be extended to test the performance of other minor-embedding algorithms. Lastly, a valuable future measurement would be to compare the running time of different embedding algorithms.

The second direction of future research involves exploring novel embedding strategies, including modifications based on Minorminer, as discussed in [22] and [23], as well as entirely different approaches to the problem, such as those presented in [24], [26], [25], and [43]. Potential straightforward ideas derived from this investigation for developing new methods include:

- *Utilizing a combination of CE and Minorminer to embed problems:* An example of this approach can be seen in [23], where the authors propose initializing an embedding with CE and then refining it with Minorminer as a local search improvement method.
- *Enhancing solution quality through multiple executions of Minorminer:* Based on the variability of Minorminer’s results illustrated in Figure 8, there are certain problems where the algorithm exhibits high instability. In these cases, executing Minorminer multiple times can significantly enhance the final solution’s quality. Although multiple executions require more time, they could be performed in parallel, if feasible.

- *Modifying Minorminer to a problem-aware algorithm:* This process involves considering the weight of variables and interactions for minor-embedding. For example, it may include embedding variables with a higher impact on solution energy into shorter chains, with the objective of prioritizing the accurate assessment of these high-impact variables during problem-solving. Even if this idea does not necessarily lead to better results on ACL of embeddings, it could lead to a lower impact of ACL on the final performance of the annealer.

Beyond the strategies mentioned above, this work justifies both previous and future efforts to develop better minor-embedding solutions. Moreover, we encourage other teams to consider this work not only when designing new minor-embedding algorithms but also when developing problem partitioning techniques, new hybrid algorithms, or related methodologies.

Acknowledgements

This work was supported by the Basque Government through Plan complementario comunicación cuántica (EXP. 2022/01341) (A/20220551) and the BIKAINTEK PhD support program. During the preparation of this work, the authors used Microsoft Copilot to improve the language and readability of the manuscript. After using this tool/service, the authors reviewed and edited the content as needed, taking full responsibility for the content of the publication.

References

- [1] J. Preskill, Quantum computing in the nisq era and beyond, *Quantum* 2 (2018) 79.
- [2] A. Peruzzo, J. McClean, P. Shadbolt, M.-H. Yung, X.-Q. Zhou, P. J. Love, A. Aspuru-Guzik, J. L. O’Brien, A variational eigenvalue solver on a photonic quantum processor, *Nature communications* 5 (1) (2014) 4213.
- [3] E. Farhi, J. Goldstone, S. Gutmann, A quantum approximate optimization algorithm, *arXiv preprint arXiv:1411.4028* (2014).
- [4] D-Wave Developers, D-Wave Hybrid Solver Service: An Overview, Tech. Rep. 14-1039A-B, D-Wave Systems Inc. (05 2020).
- [5] D. A. Lidar, T. A. Brun, *Quantum error correction*, Cambridge university press, 2013.
- [6] Z. Cai, R. Babbush, S. C. Benjamin, S. Endo, W. J. Huggins, Y. Li, J. R. McClean, T. E. O’Brien, Quantum error mitigation, *Reviews of Modern Physics* 95 (4) (2023) 045005.
- [7] E. Farhi, J. Goldstone, S. Gutmann, M. Sipser, Quantum computation by adiabatic evolution, *arXiv preprint quant-ph/0001106* (2000).
- [8] A. Messiah, *Quantum mechanics*, Volume II, Elsevier Science, Amsterdam, 1961.
- [9] A. W. Glaetzle, R. M. van Bijnen, P. Zoller, W. Lechner, A coherent quantum annealer with rydberg atoms, *Nature communications* 8 (1) (2017) 15813.
- [10] D. Raventós, T. Graß, B. Juliá-Díaz, M. Lewenstein, Semiclassical approach to finite-temperature quantum annealing with trapped ions, *Physical Review A* 97 (5) (2018) 052310.
- [11] M. W. Johnson, M. H. Amin, S. Gildert, T. Lanting, F. Hamze, N. Dickson, R. Harris, A. J. Berkley, J. Johansson, P. Bunyk, et al., Quantum annealing with manufactured spins, *Nature* 473 (7346) (2011) 194–198.
- [12] D.-W. S. Inc., Getting started with the d-wave system, accessed: 2025-02-17 (n.d.). URL https://docs.dwavesys.com/docs/latest/doc_getting_started.html

- [13] F. Glover, G. Kochenberger, Y. Du, A tutorial on formulating and using qubo models, arXiv preprint arXiv:1811.11538 (2018).
- [14] A. Lucas, Ising formulations of many np problems, *Frontiers in physics* 2 (2014) 5.
- [15] B. Tasseff, T. Albash, Z. Morrell, M. Vuffray, A. Y. Lokhov, S. Misra, C. Coffrin, On the emerging potential of quantum annealing hardware for combinatorial optimization, *Journal of Heuristics* 30 (5) (2024) 325–358.
- [16] H. M. Bauza, D. A. Lidar, Scaling advantage in approximate optimization with quantum annealing, arXiv preprint arXiv:2401.07184 (2024).
- [17] N. Mohseni, P. L. McMahon, T. Byrnes, Ising machines as hardware solvers of combinatorial optimization problems, *Nature Reviews Physics* 4 (6) (2022) 363–379.
- [18] D. Willsch, M. Willsch, C. D. Gonzalez Calaza, F. Jin, H. De Raedt, M. Svensson, K. Michielsen, Benchmarking advantage and d-wave 2000q quantum annealers with exact cover problems, *Quantum Information Processing* 21 (4) (2022) 141.
- [19] P. I. Bunyk, E. M. Hoskinson, M. W. Johnson, E. Tolkacheva, F. Altomare, A. J. Berkley, R. Harris, J. P. Hilton, T. Lanting, A. J. Przybysz, et al., Architectural considerations in the design of a superconducting quantum annealing processor, *IEEE Transactions on Applied Superconductivity* 24 (4) (2014) 1–10.
- [20] J. Cai, W. G. Macready, A. Roy, A practical heuristic for finding graph minors (2014).
- [21] T. Boothby, A. D. King, A. Roy, Fast clique minor generation in chimera qubit connectivity graphs, *Quantum Information Processing* 15 (2016) 495–508.
- [22] J. P. Pinilla, S. J. E. Wilton, Layout-aware embedding for quantum annealing processors, in: M. Weiland, G. Juckeland, C. Trinitis, P. Sadayappan (Eds.), *High Performance Computing*, Springer International Publishing, Cham, 2019, pp. 121–139.
- [23] S. Zbinden, A. Bärtschi, H. Djidjev, S. Eidenbenz, Embedding algorithms for quantum annealers with chimera and pegasus connection topologies, in: P. Sadayappan, B. L. Chamberlain, G. Juckeland, H. Ltaief (Eds.), *High Performance Computing*, Springer International Publishing, Cham, 2020, pp. 187–206.
- [24] Y. Sugie, Y. Yoshida, N. Mertig, T. Takemoto, H. Teramoto, A. Nakamura, I. Takigawa, S.-I. Minato, M. Yamaoka, T. Komatsuzaki, Graph minors from simulated annealing for annealing machines with sparse connectivity, in: D. Fagan, C. Martín-Vide, M. O’Neill, M. A. Vega-Rodríguez (Eds.), *Theory and Practice of Natural Computing*, Springer International Publishing, Cham, 2018, pp. 111–123.
- [25] T. D. Goodrich, B. D. Sullivan, T. S. Humble, Optimizing adiabatic quantum program compilation using a graph-theoretic framework, *Quantum Information Processing* 17 (2018) 1–26.
- [26] D. E. Bernal, K. E. C. Booth, R. Dridi, H. Alghassi, S. Tayur, D. Venturelli, Integer programming techniques for minor-embedding in quantum annealers, in: E. Hebrard, N. Musliu (Eds.), *Integration of Constraint Programming, Artificial Intelligence, and Operations Research*, Springer International Publishing, Cham, 2020, pp. 112–129.
- [27] E. Osaba, P. Miranda-Rodríguez, D-wave’s nonlinear-program hybrid solver: Description and performance analysis, *IEEE Access* (2025).
- [28] S. Yarkoni, E. Raponi, T. Bäck, S. Schmitt, Quantum annealing for industry applications: Introduction and review, *Reports on Progress in Physics* 85 (10) (2022) 104001.
- [29] J. Matoušek, R. Thomas, On the complexity of finding iso-and other morphisms for partial k-trees, *Discrete Mathematics* 108 (1-3) (1992) 343–364.
- [30] N. Robertson, P. D. Seymour, Graph minors. xiii. the disjoint paths problem, *Journal of combinatorial theory, Series B* 63 (1) (1995) 65–110.
- [31] K. Boothby, P. Bunyk, J. Raymond, A. Roy, Next-generation topology of d-wave quantum processors, arXiv preprint arXiv:2003.00133 (2020).
- [32] K. Boothby, A. D. King, J. Raymond, Zephyr Topology of D-Wave Quantum Processors (2021).
- [33] A. Hagberg, P. J. Swart, D. A. Schult, Exploring network structure, dynamics, and function using networkx, Tech. rep., Los Alamos National Laboratory (LANL), Los Alamos, NM (United States) (2008).
- [34] R. M. Karp, *Reducibility among combinatorial problems*, Springer, 2009, pp. 219–241.
- [35] E. Lobe, A. Lutz, Minor embedding in broken chimera and derived graphs is np-complete, *Theoretical Computer Science* 989 (2024) 114369.
- [36] P. Erdős, A. Rényi, On random graphs i, *Publ. math. debrecen* 6 (290-297) (1959) 18.
- [37] G. Palubeckis, Multistart tabu search strategies for the unconstrained binary quadratic optimization problem, *Annals of Operations Research* 131 (2004) 259–282.
- [38] S. Kirkpatrick, C. D. Gelatt Jr, M. P. Vecchi, Optimization by simulated annealing, *science* 220 (4598) (1983) 671–680.
- [39] T. Zaborniak, R. de Sousa, Benchmarking hamiltonian noise in the d-wave quantum annealer, *IEEE Transactions on Quantum Engineering* 2 (2021) 1–6.
- [40] A. Rajak, S. Suzuki, A. Dutta, B. K. Chakrabarti, Quantum annealing: An overview, *Philosophical Transactions of the Royal Society A* 381 (2241) (2023) 20210417.
- [41] E. Pelofske, G. Hahn, H. N. Djidjev, Noise dynamics of quantum annealers: estimating the effective noise using idle qubits, *Quantum Science and Technology* 8 (3) (2023) 035005.
- [42] A.-L. Barabási, R. Albert, Emergence of scaling in random networks, *science* 286 (5439) (1999) 509–512.
- [43] H. M. Ngo, N. H. K. Do, M. N. Vu, T. Kahveci, M. T. Thai, Charm: A chain-based reinforcement learning approach for the minor embedding problem (2024).